Journal of Power Sources 250 (2014) 188–195

Contents lists available at ScienceDirect

Journal of Power Sources

journal homepage: www.elsevier.com/locate/jpowsour

Cobalt-free polycrystalline $Ba_{0.95}La_{0.05}FeO_{3-\delta}$ thin films as cathodes for intermediate-temperature solid oxide fuel cells

Dengjie Chen [a], Chi Chen [a], Feifei Dong [b], Zongping Shao [b], Francesco Ciucci [a,c,*]

[a] Department of Mechanical and Aerospace Engineering, The Hong Kong University of Science and Technology, Clear Water Bay, Kowloon, Hong Kong, China
[b] State Key Laboratory of Materials-Oriented Chemical Engineering, College of Chemistry & Chemical Engineering, Nanjing University of Technology, No. 5 Xin Mofan Road, Nanjing, 210009, China
[c] Department of Chemical and Biomolecular Engineering, The Hong Kong University of Science and Technology, Clear Water Bay, Kowloon, Hong Kong, China

HIGHLIGHTS

- $Ba_{0.95}La_{0.05}FeO_{3-\delta}$ polycrystalline thin films are fabricated by PLD.
- Performance of thin films with different current collectors is evaluated.
- A polarization resistance of 0.437 Ω cm^2 at 700 °C and 0.21 atm is achieved.
- Two main oxygen reduction reaction processes determine the overall reaction.

ARTICLE INFO

Article history:
Received 21 September 2013
Received in revised form
4 November 2013
Accepted 8 November 2013
Available online 18 November 2013

Keywords:
Pulsed laser deposition
Barium ferrite compound
Mixed ionic and electronic conductor
Thin film
Solid oxide fuel cells
Electrochemical impedance spectroscopy

ABSTRACT

$Ba_{0.95}La_{0.05}FeO_{3-\delta}$ (BLF) thin films as electrodes for intermediate-temperature solid oxide fuel cells are prepared on single-crystal yttria-stabilized zirconia (YSZ) substrates by pulsed laser deposition. The phase structure, surface morphology and roughness of the BLF thin films are characterized by X-ray diffraction, scanning electron microscopy and atomic force microscopy. X-ray photoelectron spectroscopy is used to analyze the compositions of the deposited thin film and the chemical state of transition metal. The dense thin film exhibits a polycrystalline perovskite structure with a low surface roughness and a high oxygen vacancy concentration on the surface. Ag (paste or strip) and Au (strip) are applied on both surfaces of the symmetric cells as current collectors to evaluate electrochemical performance of the thin films. The electrode polarization resistances of the symmetric cells are found to be lower than those of most cobalt-free thin-film electrodes, e.g., 0.437 Ω cm^2 at 700 °C and 0.21 atm. The oxygen reduction reaction mechanism of the BLF cathode in symmetric cells is studied by electrochemical impedance spectroscopy thanks to the equivalent fitting analysis. Both the oxygen surface exchange reaction and charge transfer are shown to determine the overall oxygen reduction reaction.

1. Introduction

Perovskite-type mixed ionic and electronic conductors (MIECs) have been widely applied in solid oxide fuel cells (SOFCs) and in some related technologies [1–6], including electrolysis devices, gas sensors, batteries, oxygen transport membranes and so on, since the properties of perovskites can be easily tailored by doping/substituting ions to meet given requirements. Intermediate-temperature SOFCs (IT-SOFCs) have attracted a great deal of attention as potential power generators because of the high efficiency, low environmental impact and fuel versatility. Among many perovskite-type MIEC materials, Co-based MIECs usually show high electro-catalytic activities, excellent oxygen transport and surface exchange properties and consequently high electrochemical activities [7–14]. The practical application of theses Co-based MIECs, however, are questionable when considering their stability and thermal expansion of such materials as well as the cost of Co and other rare metals [15,16]. Thus, Fe-based MIECs are considered as potential alternatives because of the increased thermal stability and lower price. Several Fe-based MIECs have been developed as potential cathodes for IT-SOFCs [17–27], For example, $La_xSr_{1-x}FeO_{3-\delta}$, $Ba_{0.5}Sr_{0.5}Zn_{0.2}Fe_{0.8}O_{3-\delta}$, $LnBaFe_2O_{5+\delta}$, $Bi_{0.5}Sr_{0.5}FeO_{3-\delta}$ (BSF), $Sr_{0.9}K_{0.1}FeO_{3-\delta}$ and $Ba_{0.95}La_{0.05}FeO_{3-\delta}$ (BLF) perovskite oxides as

* Corresponding author. Department of Chemical and Biomolecular Engineering, The Hong Kong University of Science and Technology, Clear Water Bay, Kowloon, Hong Kong, China. Tel.: +852 2358 7187.
E-mail addresses: mefrank@ust.hk, francesco.ciucci@gmail.com (F. Ciucci).

0378-7753/$ – see front matter © 2013 Elsevier B.V. All rights reserved.
http://dx.doi.org/10.1016/j.jpowsour.2013.11.010

well as their derivatives have been reported with reasonable electro-catalytic activities for oxygen reduction as well as the good operational stability.

Among them, micro-sized BLF cathodes with a porous structure showed encouraging stability and electrochemical performance, which is comparable at intermediate temperatures to Co-based $Ba_{0.5}Sr_{0.5}Co_{0.8}Fe_{0.2}O_{3-\delta}$ (BSCF) [7]. The electrode polarization resistances (R_p) as low as 0.037 Ω cm^2 at 700 °C has been obtained using porous thick film electrodes [18]. In addition, stable R_p at 700 °C within a total test period of 1200 h and stable power outputs at a constant polarization current density indicated that the practical application feasibility of the BLF cathode [18]. In addition, BLF oxygen transport membranes for oxygen separation from air show a high oxygen permeation flux [28–30].

For practical applications, the cathode layer of an SOFC should be porous in order to enhance gas transportation and provide more active sites for oxygen reduction reactions (ORR). Since the microstructure cannot be controlled with significant precision, it is difficult to rigorously explore the electrochemical properties of such porous cathodes. In order to simplify the morphological complexities and gain a better understanding on the ORR mechanism, thin-film electrode should be employed. In addition, a reliable R_p value of the BLF for comparison and evaluation is still lacking in the literature. The BLF thin films are prepared and evaluated experimentally under oxidizing conditions. The ORR mechanism of the BLF thin-film electrode is also discussed.

2. Experimental

2.1. Sample preparation

2.1.1. Powder and target

The BLF powders for the target were prepared by a combined EDTA-citrate complexing process [18]. Precursors of nitrates, $Ba(NO_3)_2$, $La(NO_3)_3$ and $Fe(NO_3)_3$ (all in A.R. grade, Sinopharm Chemical Reagent Co. Ltd) were applied as raw materials for the cation sources. The exact bonding of the water in the nitrates was determined by standard EDTA titration method. According to the nominal composition, stoichiometric amounts of the above nitrates were dissolved in deionized water at 90 °C. Both EDTA and citric acid (CA) used as the complexing agents were added into the solution based on the molar ratio of total cations, EDTA and CA in the solution as 1:1:2. The pH value of the aqueous solution was maintained to ~6 by adding NH_3 aqueous solution during the evaporation process to avoid any precipitation of individual cations in the solution. Then the temperature was adjusted to 120 °C with stirring to evaporate water until a viscous and transparent gel appeared. The gel was subsequently shifted to an oven at 250 °C for 6 h to produce a gray solid precursor with network structure. The obtained solid precursor was finally calcined in muffle furnace at 1000 °C for 5 h in air atmosphere to remove the carbon and form powders with the pure phase BLF structure.

Dense BLF targets for pulsed laser deposition (PLD) with ~2 mm in thickness were prepared through dry pressing the as-synthetized powders by a 15 mm (diameter) stainless steel mold at a hydraulic pressure of ~20 MPa. The disk-type green samples were then sintered at 1200 °C for 10 h under stagnant air to obtain a dense target. The target was then polished on both faces before used for PLD.

2.1.2. Thin film

The BLF thin-film electrodes were deposited on both sides of a 10 × 10 × 0.5 mm single-crystal 8 mol.% Y_2O_3-stabilized ZrO_2 (YSZ, (001) orientation, $a = b = c = 5.125$ Å, MTI) substrate by PLD (Neocera JP-788) with a Nd:YAG laser (Continuum Surelite SLIII-10) at quadrupled wavelength of 266 nm. The PLD chamber was pumped down to a typical background pressure of ~9 × 10^{-6} mTorr before heating the substrate. The deposition of BLF was performed at an oxygen partial pressure of 160 mTorr and the target was ablated by laser beam with an energy density of about ~5 J cm^{-2}. After deposition, the sample was annealed at 600 °C for 1 h, 700 °C for 45 min or 800 °C for 15 min under an oxygen partial pressure of 200 Torr at corresponding depositing temperature. The heating and cooling rate of the substrate was controlled at 10 °C min^{-1}.

2.2. Characterization

2.2.1. Structure characterization

The phase structure of the deposited thin film was determined by X-ray diffraction (XRD, PANalytical). The patterns were recorded at room temperature in the 2θ range of 20–80° using Cu Kα radiation (λ = 1.5406 Å) with a scanning step of 0.06°. The microstructures of the deposited BLF thin films were recorded using a field-emission scanning electron microscope (SEM, JSM-6700F) operating at 5.0 kV. An Au conductive layer was coated on the thin-film surface for SEM observation. Atomic force microscopy (AFM, Nanoscope IIIa/Dimension 3100) was used to record the roughness and surface morphologies of thin films under tapping mode with the scan rate of 0.5 Hz and with 512 number of samples/lines. The elements and chemical valence state of the prepared samples was analyzed by X-ray photoelectron spectroscopy (XPS, PHI 5600) with Al monochromatic X-ray at a power of 150 W.

2.2.2. Electrochemical impedance spectroscopy

Symmetric cells with two electrodes were used to determine the polarization resistances. Electrochemical impedance spectroscopy (EIS) was carried out using an electrochemical workstation (VSP, Bio-Logic) between 550 and 700 °C at various oxygen partial pressures (0.04–1 atm) using mass flow controllers. The frequency range of 10^{-1}–2 × 10^5 Hz with an amplitude AC voltage of 10 mV was applied under open circuit voltage conditions. A suitable equivalent circuit with the ZView 2.9 (Scribner Associates) software program was used to fit EIS results.

3. Results and discussion

3.1. Phase and microstructure

The crystalline phase of the deposited BLF thin film was characterized by XRD since the phase structure of the thin film may have a great influence on materials properties [18]. Shown in Fig. 1 are XRD patterns of the BLF thin films deposited on the YSZ (001) substrates. Other than the sample annealed at 600 °C with the detection of some impurities or secondary phases, the XRD patterns obtained from the other two BLF thin films are in good agreement with the bulk BLF XRD data with a cubic perovskite structure, suggesting a cubic polycrystalline nature [18]. No preferred orientations in the thin-film growth are observed because of the substantial lattice mismatch between the BLF (a = 4.0051 Å) [18] and YSZ (a = 5.125 Å) and because of the deposition conditions. No characteristic reflections of secondary phases or insulating phases are detected within three investigated samples, suggesting the chemical instability between the BLF thin film and the YSZ substrate is negligible within the investigated annealing temperatures. It is also found that the crystallinity of the BLF samples was similar at all different annealing temperatures.

Typical SEM surface morphologies and a cross-sectional image of the polycrystalline BLF thin films deposited on the YSZ electrolytes with different annealing temperatures are displayed in Fig. 2.

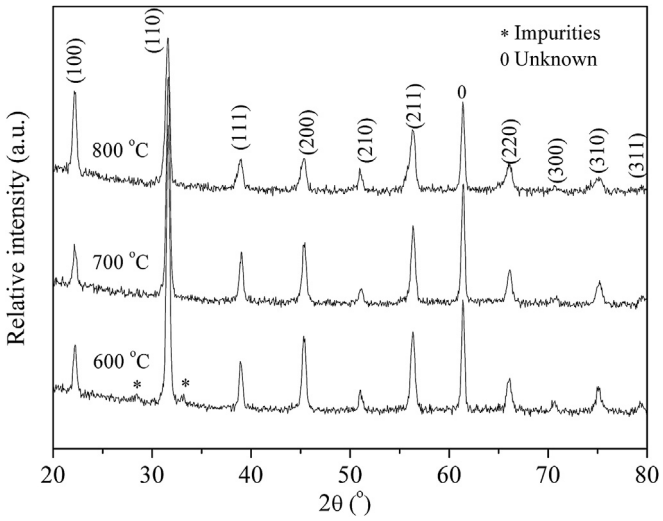

Fig. 1. XRD patterns of the BLF thin films deposited on YSZ (001) substrates at 600, 700 and 800 °C. The unknown peak is not from the BLF material itself.

Distinctive microstructures can be observed with different annealing temperatures. The grains are observed for all films due to the lattice mismatch between the BLF thin film and the YSZ substrate. In the case of the thin film annealed at 800 °C, some cracks and coarse particles are observed. Dense, continuous and crack-free microstructures with no abnormal grain growth of the BLF thin films are obtained at the annealing temperature of 700 °C. At a lower temperature of 600 °C, it can be noted that the structure is somewhat porous and the grains are not well-defined. A dense layer with the thickness of ~200 nm and a good adhesion between the YSZ electrolyte and the deposited BLF thin film are observed from the cross-sectional image with the sample annealed at 700 °C. Considering the surface morphology, annealing temperature of 700 °C is chosen. Therefore it can be expected that the electrochemical performance may entirely originate from the material itself with no influence of the porous microstructure.

The surface morphology of the BLF thin film was also investigated by AFM. In Fig. 3, a typical 3D AFM image of the BLF thin films annealed at 700 °C for 45 min is presented. The height scale can refer to the dark to bright contrast color (40 nm per interval). The thin film shows well-defined grains on surface. The root mean square (rms) surface roughness of 1.957 nm is determined for an area of ~2 × 2 μm^2. Though the deposited thin film is polycrystalline, the well-defined grains and narrow distributions of gains are confirmed. This result further indicates that the actual active area for electrocatalysis nears the nominal one (10 × 10 mm^2).

The composition and surface valence state of the Fe ion in polycrystalline BLF thin film deposited on the YSZ substrate were determined by XPS at room temperature. As shown in Fig. 4, XPS spectrum indicates same elements (Ba, La, Fe and O) except C as that in the target sample. The atomic ratio of 0.46 for [Fe]/([Fe] + [Ba] + [La]) is obtained, which is reasonably close to the ideal values. It has to be pointed out that the composition in the near-surface region may be somewhat different when compared to the overall elements distribution in the thin film and target materials. Shown in Fig. 4b is the typical asymmetric Fe 2p core level spectra, which consists of the doublet peaks with the binding energies of 710.7 and 723.9 eV can be assigned to be Fe $2p_{3/2}$ and Fe $2p_{1/2}$, respectively. It has been detected that the binding energy difference of 13.2 and 13.6 eV was assigned to metallic Fe and Fe_2O_3, respectively [31]. The obtained binding energy difference for Fe $2p_{1/2}$ and Fe $2p_{3/2}$ peaks are larger than those of Fe^{3+}, suggesting the peak at least consists of Fe^{2+}, Fe^{3+} and Fe^{4+}. By curve-fitting of the Fe $2p_{3/2}$ peak as an example, three Fe components, including Fe^{2+} (19.04%), Fe^{3+} (48.69%) and Fe^{4+} (32.26%) are confirmed from the sum of the these peaks fitted well of the experimental peak, resulting in the average valence of 3.13. According to the electroneutrality principle and the assumption that the nominal stoichiometry of the BLF composition is Ba:La:Fe = 0.95:0.05:1, the oxygen vacancy concentration (δ) of 0.409 is derived, which is fairly similar

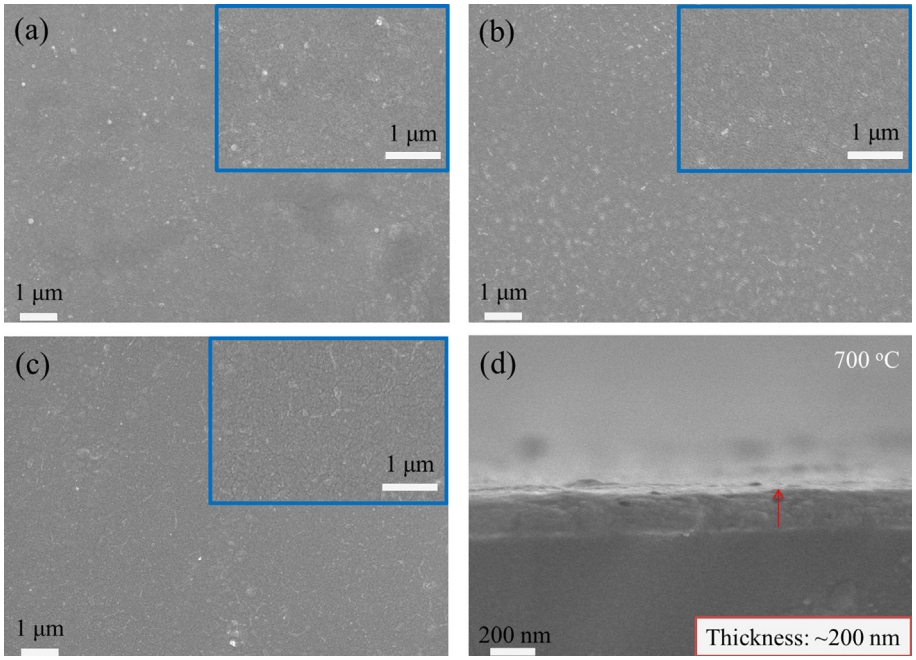

Fig. 2. Surface SEM images of the polycrystalline BLF thin film deposited on YSZ electrolyte with different annealing temperatures at 600 °C (a), 700 °C (b) and 800 °C (c), as well as the cross-sectional image of the thin film after annealed at 700 °C (d). Insides are the images with large magnifications.

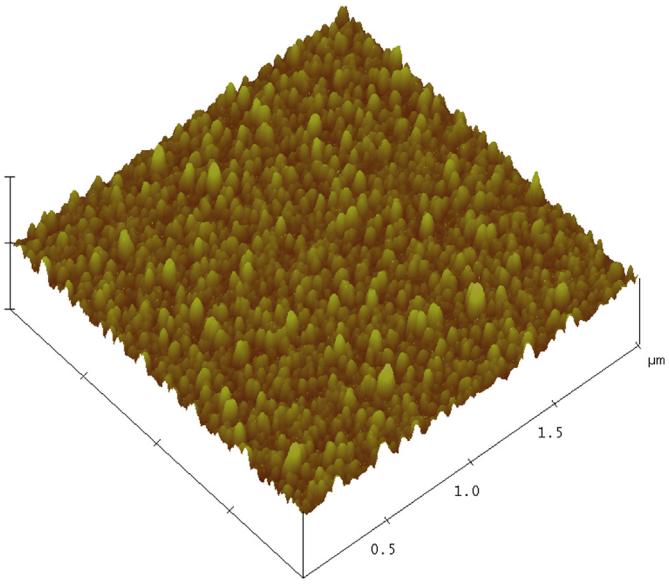

Fig. 3. A typical 3D AFM image of the BLF thin film annealed at 700 °C for 45 min.

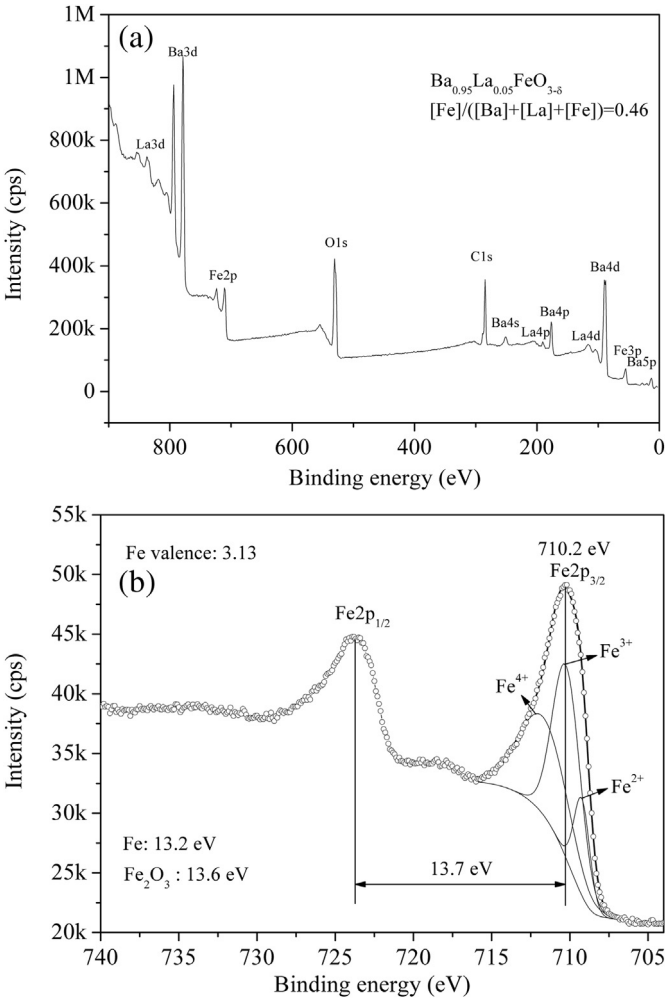

Fig. 4. A survey spectrum of the BLF thin film (a) and a high-resolution spectrum of the asymmetric Fe 2p core level.

to the value from the BLF power materials determined by iodometric titration at room temperature in the previous report [18]. The high δ value will be beneficial to the ORR.

3.2. Electrochemical impedance spectroscopy

It is well recognized that a better understanding of the intrinsic ORR mechanism can guide the design of highly active electrode materials at intermediate temperatures [32,33]. For traditional porous MIEC cathodes, ORR ($O_2 + 4e^- + 2V_{\dot{O}} \rightarrow 2O_O^x$) on cathodes include complex processes that may comprise several individual steps and sub-steps: (i) gas diffusion of oxygen through pores of the porous cathode layer, (ii) surface diffusion of oxygen ad-molecules, (iii) adsorption and dissociation of oxygen molecules into two oxygen atoms on the entire active surface, (iv) incorporation of the oxygen atoms into oxygen vacancies, (v) oxygen ions transfer inside the bulk and between grain interfaces and (vi) charge transfer of oxygen ions into oxygen-ionic electrolyte [32,34–37]. In contrast to the porous cathode, steps i, ii and v can be neglected in the dense thin film cathode considering the restricted active surface area and small film thickness. The process iii and iv can be considered together as the oxygen surface reaction process. Therefore, the investigation of the intrinsic ORR mechanism of BLF electrode will be much easier and reliable with the thin-film electrode.

To determine the ORR rate-limiting steps in the electrode, the EIS under different temperatures and oxygen partial pressures were conducted. The electrode polarization resistances (R_p) of the cells in this report are all adjusted to the nominal surface area (1 cm^2). The R_p of the symmetric cells (Ag paste/BLF/YSZ/BLF/Ag paste) at 550–700 °C under the oxygen partial pressures of 0.04–1 atm are plotted in Fig. 5. The increase of the R_p is observed when decreasing oxygen partial pressure and temperature. The activation energies (E_a) of the BLF electrode under various oxygen partial pressures are determined from the Arrhenius plot as shown in Fig. 5. E_a of 89.3, 87.9, 88.0, 87.4, 86.4, 84.8 and 83.2 kJ mol^{-1} for BLF for various oxygen partial pressures is relatively low compared to other cobalt-free cathodes (e.g. 133 kJ mol^{-1} for $SrNb_{0.1}Fe_{0.9}O_{3-\delta}$ and 117 kJ mol^{-1} for BSF) or other thin-film cathodes (e.g. 119 kJ mol^{-1} for $La_{0.5}Sr_{0.5}CoO_{3-\delta}$) [23,38,39]. This E_a is even lower than the E_a measured for porous BLF electrodes, but it is comparable to the activation energy of the chemical diffusion and surface exchange of

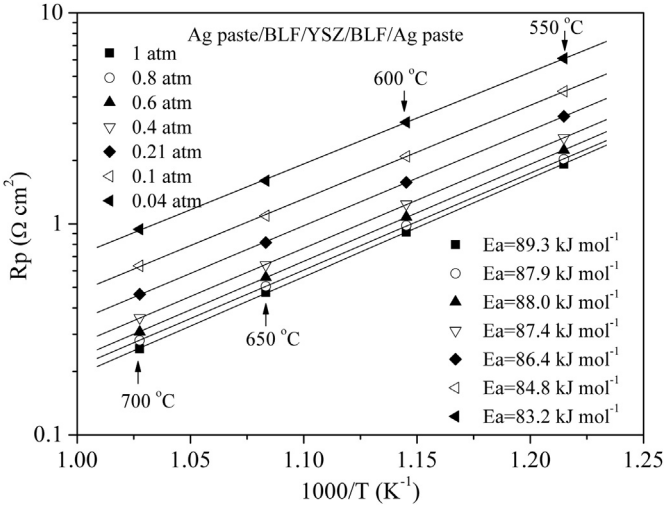

Fig. 5. Temperature dependence (550–700 °C) of the R_p values for the symmetric cells with the BLF/YSZ/BLF configuration under open circuit conditions at oxygen partial pressures of 0.04–1 atm.

dense BLF sample [18]. The low E_a may be due to the high oxygen reduction activity of the nanoscaled cathode even at low temperatures, which is beneficial to IT-SOFCs. The low E_a at low oxygen partial pressures indicates that the oxygen reduction activity increases with increasing oxygen vacancy concentration. In a symmetric cell setting (Ag paste/BLF/YSZ/BLF/Ag paste) the typical R_p for this thin film is 0.465 Ω cm^2 at 700 °C at air conditions. For comparison, surface resistance (R_s) values of the other typical cathodes reported in literature are also given in Fig. 6. R_p of the as-deposited thin film is one order of magnitude higher than the reported R_p of the porous BLF cathode with the same composition [18]. The obtained results are encouraging since the actual active surface area for oxygen reduction of a porous electrode with mixed conductivity is typically one order of magnitude larger than the corresponding property of the dense electrode. In addition, the reported R_p values are comparable to or lower than the other reported electrodes when only the dense thin film is adopted as the cathode [27,40–44]. For example, R_s of ~0.260 Ω cm^2 was obtained from BSCF, R_s of 2.60 Ω cm^2 for $Sm_{0.5}Sr_{0.5}CoO_{3-\delta}$ in a microelectrode configuration at 700 °C as reported by Baumann and coworkers [41,42]. Though some thin-film cathodes have been reported to have extremely low R_p values, it should be pointed out that in their configurations either a porous layer with the same composition of the dense thin film was applied as the current collector or nanocrystalline thin film with extremely high surface area was used [39,45]. The electrochemical performance comparison also reveals that BLF is an extremely promising candidate for intermediate or low temperature SOFCs.

Shown in Fig. 7a are representative EIS of the BLF/YSZ/BLF symmetrical cell under oxygen partial pressures ranging from 0.04 to 1 atm at 700 °C under OCV conditions. In the Nyquist plots of the EIS, each ORR process may be characterized by frequencies and at least two primary chemical–physical processes control the overall ORR in the thin-film electrode. Therefore, arcs located at high frequency (HF) and a low frequency (LF) in the Nyquist plots represented two main ORR processes are used to analyze the ORR characteristics. As observed, oxygen partial pressures have no significant effect on the HF arc, but are likely to be more influential on the LF arc. To further clarify the contributions of the each electrode process, the equivalent circuit of Fig. 7b is adopted to fit the EIS data, where (R-CPE) represents the processes occurred at HF and LF

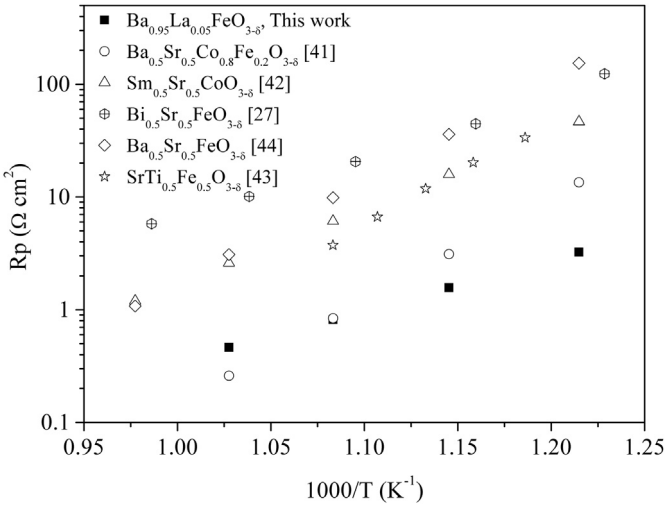

Fig. 6. A comparison of R_p values of the BLF cathode to other typical cathodes reported in literature. Only the surface resistance (R_s) of the materials is extracted from the reported results for comparison.

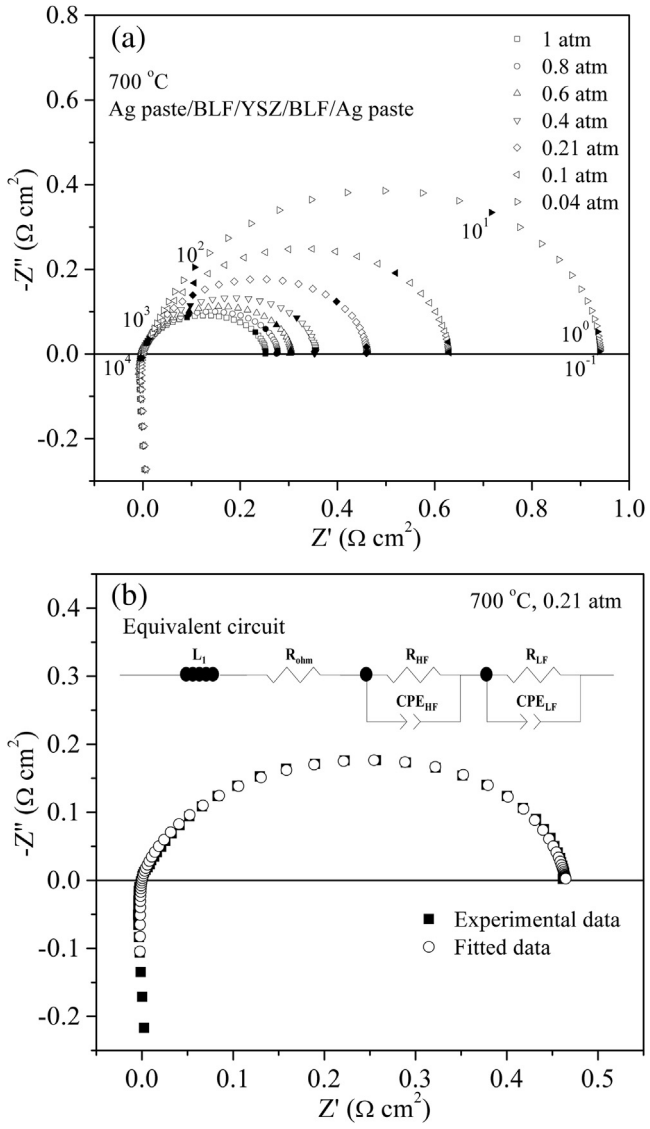

Fig. 7. EIS of the BLF/YSZ/BLF symmetric cell measured at 700 °C as a function of oxygen partial pressure (a) and a representative EIS with the experimental data (solid squares) and fitted data (open circles) based on a suitable equivalent circuit at 700 °C and 0.21 atm (b).

regions, respectively, L is the induction tail due to the device and wiring and R_{ohm} corresponds to the ohmic resistance of the cell. The CPE represents a constant phase element which assumes that the seen chemical or double layer capacitance is non-ideal. Neither Warburg nor Gerischer elements can represent the LF arc, thus R-CPE elements are selected. Fig. 7b presents a representative EIS with the measured and fitted data, and it highlights that the fitting error residuals are typically small.

It has been reported that each elemental process of the ORR over mixed ionic and electronic conducting electrodes displays a unique dependence on the pO_2 [34,37,46], e.g., $1/R_p = pO_2^m$, where $m = 0.25$ usually represents that a charge transfer process and $m = 0.5$ corresponds to the process of oxygen surface reaction. It is usually difficult to distinguish the two processes in the EIS, especially when they hold a similar characteristic frequency (time constant). Presented in Fig. 8a are the R_{HF} and R_{LF} of BLF thin films as a function of the oxygen partial pressure at 650 and 700 °C. The slopes of $\ln(1/R_{HF})$ vs. $\ln(pO_2)$ and $\ln(1/R_{LF})$ vs. $\ln(pO_2)$ are 0.30–0.33 and 0.52–0.59, respectively, which can be approximately attributed to the aforementioned ORR

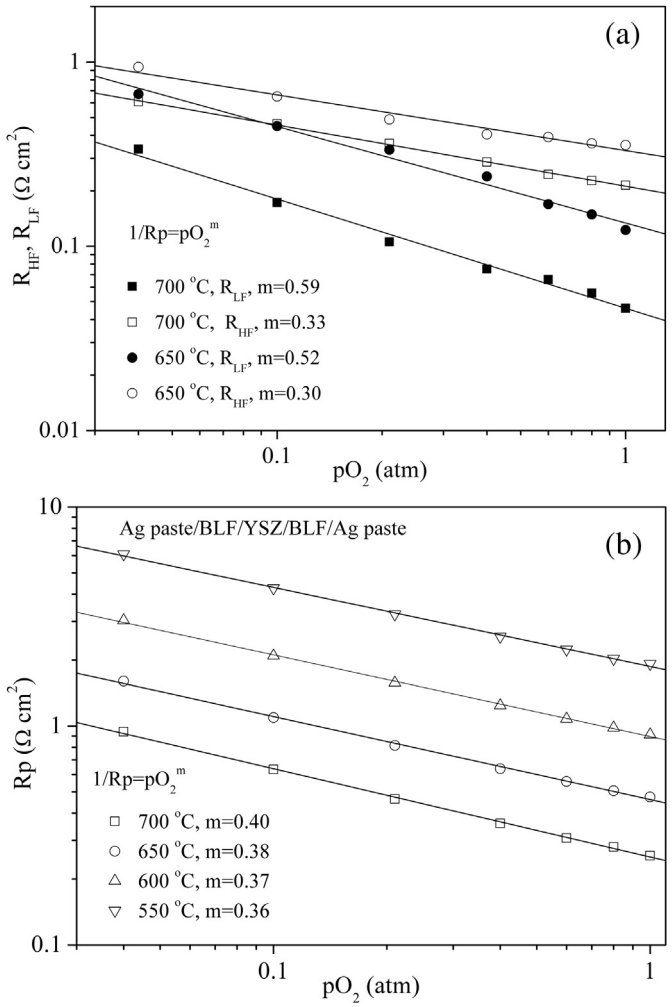

Fig. 8. pO_2 dependence of R_{HF} and R_{LF} at 650 and 700 °C (a) and $R_{HF} + R_{LF}$ at 550–700 °C (b) for the BLF thin-film cathode derived from the EIS of the BLF/YSZ/BLF symmetric cell.

mechanism. The $R_{HF} + R_{LF}$ is found to be dependent on pO_2 with the m values of 0.40, 0.38, 0.37 and 0.36 at 700, 650, 600 and 550 °C as shown in Fig. 8b, suggesting that the rate-determining step within the thin-film cathode is controlled by both surface reaction at the active surface and the charge transfer process. The m values decrease with decreasing temperature, suggesting that the charge transfer process may play a dominant role at low temperatures.

Since the stability (high-temperature evaporation, infiltration, and sintering) and electro-catalytic activity of Ag is a major concern for SOFC applications, alternative current collectors and current collecting methods were also applied. A 3.3-mm width Ag strip centered in the electrode was applied as the current collector. A 3.3-mm width Au strip was also applied as the current collector since Au is considered to be catalytically inert to oxygen. The strips were deposited by sputtering with a thickness of ~100 nm. To avoid oxidation of the nanoscaled strip, a protective layer of corresponding metal was applied to the surface of the deposited metal and subsequently annealed at 700 °C for 1 h in stagnant air. As shown in Fig. 9, by applying the Au strip as the current collector, the R_p values are only slightly larger than the cell with the Ag strip as the current collector, suggesting that the current collector material has little effect on the electrochemical performance in this current collection method. The R_p values obtained from the cells with Ag/Au strip are much larger than that with the Ag paste, which may be

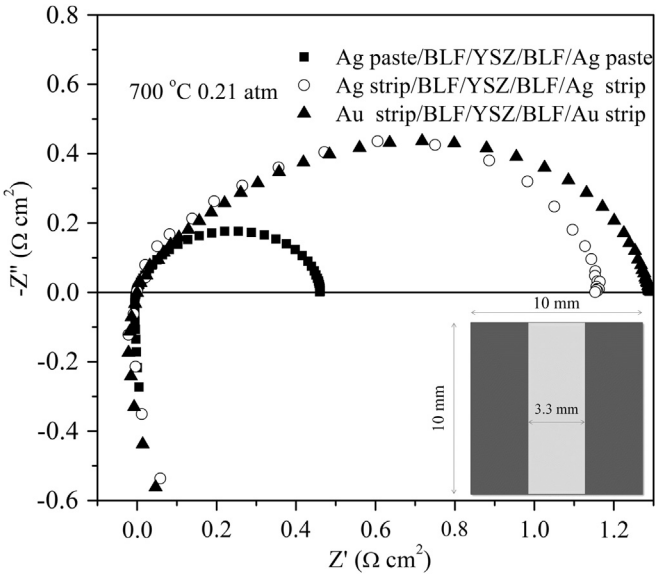

Fig. 9. Representative EIS plots with different current collectors and current collecting materials.

connected to the low electronic conductivity of the BLF material whose maximum value is approximately 11 S cm^{-1} [18]. This indicates that the current collecting method may influence the electrochemical performance; this is particularly critical when the current collectors are spaced apart and the electrocatalytic materials possess low electronic conductivity [47,48]. Meanwhile, the low price, easy operation and wide application of the Ag current collectors at relatively low temperatures, justifies the practical importance of the previous analysis, where Ag paste is used as the current collector.

Considering that some elements in BLF may react with YSZ, a $Sm_{0.2}Ce_{0.8}O_{1.9}$ (SDC) buffer layer was inserted between BLF and YSZ. A symmetric cell with BLF/SDC/YSZ/SDC/BLF configuration was prepared by PLD in order to investigate the effect of the electrolyte on the electrochemical performance. One should note, however, that the annealing temperature is lower that the temperature necessary to form the insulating phase [49] and that the XRD results in Fig. 1 do not indicate the presence of secondary phases. As shown in Fig. 10, E_a and pO_2 dependence of R_p obtained from the BLF/SDC/YSZ/SDC/BLF cell is similar to the cell without an SDC layer, suggesting the interlayer in this study is not that critical. Electrochemical performance with R_p values of 0.437, 0.800, 1.559 and 3.148 Ω cm^2 are obtained at 700, 650, 600 and 550 °C in air condition. It is observed that the R_p values of the symmetric cell with the introduction of the SDC interlayer are somewhat lower than those without the interlayer. The slightly improved R_p here may be connected to the enhanced kinetics and lower chance of the phase reaction [50,51].

4. Conclusions

The XRD, SEM and AFM results show that the deposited BLF thin film at the annealed temperature of 700 °C has polycrystalline phase structure without secondary phases and it is characterized by relatively smooth surface. Electrochemical performance of the BLF thin films is characterized in symmetric cells by EIS. Despite the relative low electronic conductivity of the BLF materials, the R_p of as-deposited thin film is lower than other common SOFC materials. The low R_p values may be linked to the relative high δ near the surface of the thin film, which is beneficial for ORR. In addition, low

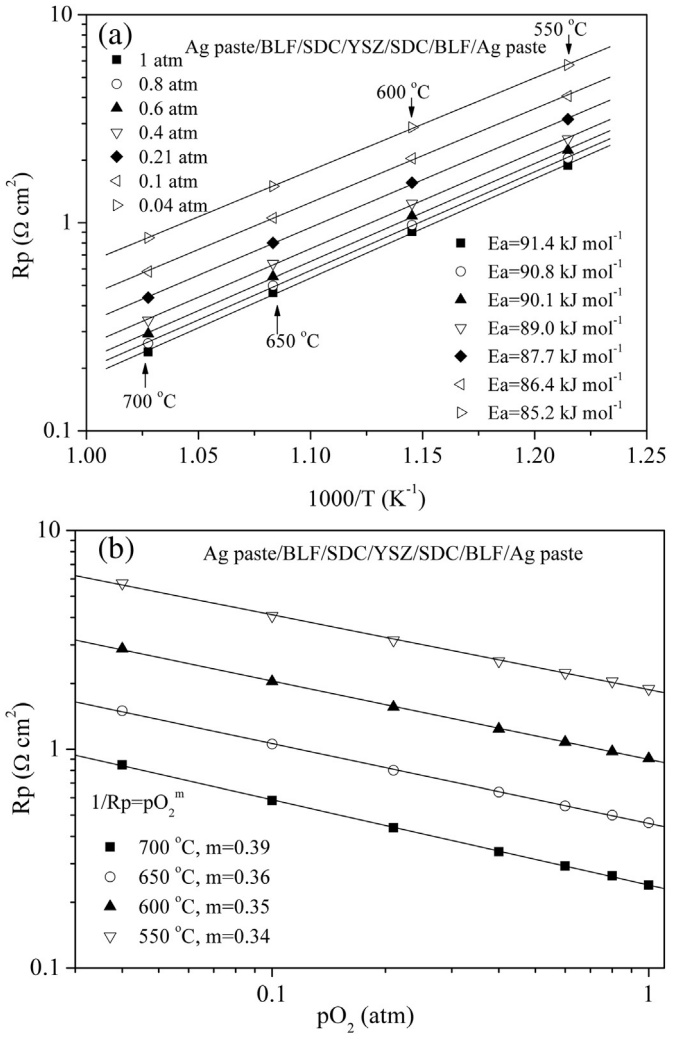

Fig. 10. Temperature dependence of the R_p values for the BLF/SDC/YSZ/SDC/BLF symmetric cell with the pO_2 in the range of 0.04–1 atm (a) and pO_2 dependence of the R_p values at 550–700 °C (b).

E_a values suggest the high oxygen reduction activity of the nano-scaled cathode at low temperatures. The thin-film cathode reactivity can be linked to both high and low frequency phenomena which may be in turn connected to surface reactions and to the charge transfer. The materials of the current collector have little effect on the electrochemical performance when the strip-type current collector is applied, while the current collecting method influences electrochemical performance considerably. The slight improvement in electrochemical performance with the BLF/SDC/YSZ/SDC/BLF cell indicates that the electrochemical performance may further be improved by modifying the interface. Future experiments will focus on fabricating BLF thin films into cathode–electrolyte–anode configuration and on testing the cell under fuel cell conditions. This material, characterized high intrinsic electrochemical performance, has potential applications in SOFCs, oxygen separation membranes, solid oxide electrolysis cells and high-temperature sensors.

Acknowledgments

F. Ciucci gratefully acknowledges the support from the grant HKUST DAG12EG06 and DAG12EG07-12. This work was also partially supported by the "National Science Foundation for Distinguished Young Scholars of China" under contract No. 51025209.

References

[1] J. Richter, P. Holtappels, T. Graule, T. Nakamura, L.J. Gauckler, Monatsh. Chem. 140 (2009) 985–999.
[2] N. Orlovskaya, N. Browning, in: Mixed Ionic Electronic Conducting Perovskites for Advanced Energy Systems: Proc. of the NATO ARW on Mixed Ionic Electronic Conducting (MIEC) Perovskites for Advanced Energy Systems, Kyiv, Ukraine, 8–12 June 2003, Springer, 2004.
[3] Y.Y. Liu, X.Y. Tan, K. Li, Catal. Rev. 48 (2006) 145–198.
[4] J. Suntivich, K.J. May, H.A. Gasteiger, J.B. Goodenough, Y. Shao-Horn, Science 334 (2011) 1383–1385.
[5] A. Kumar, F. Ciucci, D. Leonard, S. Jesse, M. Biegalski, H. Christen, E. Mutoro, E. Crumlin, Y. Shao-Horn, A. Borisevich, S.V. Kalinin, Adv. Funct. Mater. 23 (2013) 5027–5036.
[6] K. Zhang, J. Sunarso, Z.P. Shao, W. Zhou, C.H. Sun, S.B. Wang, S.M. Liu, RSC Adv. 1 (2011) 1661–1676.
[7] Z.P. Shao, S.M. Haile, Nature 431 (2004) 170–173.
[8] D.J. Chen, Z.P. Shao, Int. J. Hydrogen Energy 36 (2011) 6948–6956.
[9] W. Zhou, Z.P. Shao, R. Ran, R. Cai, Electrochem. Commun. 10 (2008) 1647–1651.
[10] C.R. Xia, W. Rauch, F.L. Chen, M.L. Liu, Solid State Ionics 149 (2002) 11–19.
[11] G.J. la O', S.J. Ahn, E. Crumlin, Y. Orikasa, M.D. Biegalski, H.M. Christen, Y. Shao-Horn, Angew. Chem. Int. Ed. 49 (2010) 5344–5347.
[12] J. Yoon, S. Cho, J.H. Kim, J. Lee, Z.X. Bi, A. Serquis, X.H. Zhang, A. Manthiram, H.Y. Wang, Adv. Funct. Mater. 19 (2009) 3868–3873.
[13] J. Liu, G. Collins, M. Liu, C. Chen, APL Mater. 1 (2013) 031101.
[14] S.L. Pang, X.N. Jiang, X.N. Li, H.X. Xu, L. Jiang, Q.L. Xu, Y.C. Shi, Q.Y. Zhang, J. Power Sources 240 (2013) 54–59.
[15] M. Arnold, T.M. Gesing, J. Martynczuk, A. Feldhoff, Chem. Mater. 20 (2008) 5851–5858.
[16] Y.B. Chen, F.C. Wang, D.J. Chen, F.F. Dong, H.J. Park, C. Kwak, Z.P. Shao, J. Power Sources 210 (2012) 146–153.
[17] D.J. Chen, F.C. Wang, H.G. Shi, R. Ran, Z.P. Shao, Electrochim. Acta 78 (2012) 466–474.
[18] F.F. Dong, D.J. Chen, Y.B. Chen, Q. Zhao, Z.P. Shao, J. Mater. Chem. 22 (2012) 15071–15079.
[19] S.P. Simner, J.R. Bonnett, N.L. Canfield, K.D. Meinhardt, J.P. Shelton, V.L. Sprenkle, J.W. Stevenson, J. Power Sources 113 (2003) 1–10.
[20] S.E. Hou, J.A. Alonso, J.B. Goodenough, J. Power Sources 195 (2010) 280–284.
[21] B. Wei, Z. Lu, X.Q. Huang, M.L. Liu, N. Li, W.H. Su, J. Power Sources 176 (2008) 1–8.
[22] Q.J. Zhou, T.M. He, Q. He, Y. Ji, Electrochem. Commun. 11 (2009) 80–83.
[23] Y.J. Niu, W. Zhou, J. Sunarso, L. Ge, Z.H. Zhu, Z.P. Shao, J. Mater. Chem. 20 (2010) 9619–9622.
[24] L.T. Yan, H.P. Ding, Z.W. Zhu, X.J. Xue, J. Power Sources 196 (2011) 9352–9355.
[25] C.J. Zhang, H.L. Zhao, J Mater. Chem. 22 (2012) 18387–18394.
[26] Q.A. Liu, X.H. Dong, G.L. Xiao, F. Zhao, F.L. Chen, Adv. Mater. 22 (2010) 5478–5482.
[27] A. Wedig, R. Merkle, B. Stuhlhofer, H.-U. Habermeier, J. Maier, E. Heifets, Phys. Chem. Chem. Phys. 13 (2011) 16530–16533.
[28] K. Watenabe, M. Yuasa, T. Kida, Y. Teraoka, N. Yamazoe, K. Shimanoe, Adv. Mater. 22 (2010) 2367–2370.
[29] T. Kida, S. Ninomiya, K. Watanabe, N. Yamazoe, K. Shimanoe, ACS Appl. Mater. Interfaces 2 (2010) 2849–2853.
[30] F.Y. Liang, K. Partovi, H.Q. Jiang, H.X. Luo, J. Caro, J. Mater. Chem. A 1 (2013) 746–751.
[31] C.D. Wagner, G.E. Muilenberg, Handbook of X-ray Photoelectron Spectroscopy: A Reference Book of Standard Data for Use in X-ray Photoelectron Spectroscopy, Physical Electronics Division, Perkin-Elmer Corp., 1979.
[32] S.B. Adler, Chem. Rev. 104 (2004) 4791–4843.
[33] A. Kumar, F. Ciucci, A.N. Morozovska, S.V. Kalinin, S. Jesse, Nat. Chem. 3 (2011) 707–713.
[34] D.J. Chen, R. Ran, Z.P. Shao, J. Power Sources 195 (2010) 4667–4675.
[35] S.B. Adler, J.A. Lane, B.C.H. Steele, J. Electrochem. Soc. 143 (1996) 3554–3564.
[36] W. Zhou, R. Ran, Z.P. Shao, J. Power Sources 192 (2009) 231–246.
[37] M.J. Escudero, A. Aguadero, J.A. Alonso, L. Daza, J. Electroanal. Chem. 611 (2007) 107–116.
[38] S.S. Jiang, W. Zhou, Y.J. Niu, Z.H. Zhu, Z.P. Shao, ChemSusChem 5 (2012) 2023–2031.
[39] S. Wang, J. Yoon, G. Kim, D. Huang, H. Wang, A.J. Jacobson, Chem. Mater. 22 (2010) 776–782.
[40] F. Baumann, J. Fleig, H. Habermeier, J. Maier, Solid State Ionics 177 (2006) 1071–1081.
[41] F. Baumann, J. Fleig, H. Habermeier, J. Maier, Solid State Ionics 177 (2006) 3187–3191.
[42] F.S. Baumann, J. Fleig, G. Cristiani, B. Stuhlhofer, H.U. Habermeier, J. Maier, J. Electrochem. Soc. 154 (2007) B931–B941.
[43] W. Jung, H.L. Tuller, J. Electrochem. Soc. 155 (2008) B1194–B1201.

[44] L. Wang, PhD thesis, Max Planck Institute for Solid State Research, 2009.
[45] L. Dieterle, P. Bockstaller, D. Gerthsen, J. Hayd, E. Ivers-Tiffee, U. Guntow, Adv. Energy Mater. 1 (2011) 249–258.
[46] M.J. Jorgensen, M. Mogensen, J. Electrochem. Soc. 148 (2001) A433–A442.
[47] F. Ciucci, Y. Hao, D.G. Goodwin, Phys. Chem. Chem. Phys. 11 (2009) 11243–11257.
[48] F. Ciucci, W.C. Chueh, D.G. Goodwin, S.M. Haile, Phys. Chem. Chem. Phys. 13 (2011) 2121–2135.
[49] D. Chen, F. Wang, Z. Shao, Int. J. Hydrogen Energy 37 (2012) 11946–11954.
[50] D. Chen, G. Yang, Z. Shao, F. Ciucci, Electrochem. Commun. 35 (2013) 131–134.
[51] Z. Fan, F.B. Prinz, Nano Lett. 11 (2011) 2202–2205.